High-resolution core-level photoemission study of dense Pb overlayers on Si(111)

Won Hoon Choi, Keun Su Kim, and Han Woong Yeom*

Center for Atomic Wires and Layers and Institute of Physics and Applied Physics, Yonsei University, Seoul 120-749, Korea
(Received 29 July 2008; published 24 November 2008)

Structure and bonding configuration of dense Pb overlayers on the Si(111) surface have been studied by low-energy-electron diffraction and high-resolution photoelectron spectroscopy using synchrotron radiation. Several representative phases in its devil's staircase phase diagram have been systematically investigated by varying the Pb coverage at 200–300 K. Pb $5d$ photoelectron spectra indicate that there exist two distinct bonding configurations of Pb, which are interpreted as the hollow and on-top (T1) sites of the structure models proposed earlier. In case of surface Si atoms, mainly two different bonding environments are revealed by surface Si $2p$ components for the low-density $\sqrt{7} \times \sqrt{3}$ phase. These can be assigned to T1 and modified on-top (T1′) sites surrounding hollow-site adatoms. As the coverage increases, the minority site T1 converts to T1′ making the topmost Si layer have a unique bonding configuration. This behavior is also consistent with the structure models. The temperature-dependent study reveals that the $\sqrt{7} \times \sqrt{3}$ phase undergoes a reversible phase transition into a 1×1 phase. This phase transition induces no significant change in Pb core levels but a marginal increase in the Si $2p$ component for the T1′ sites. We suggest a plausible scenario of the phase transition based on the structure model with 1.2 monolayer Pb and the active diffusion of hollow-site adatoms.

I. INTRODUCTION

Pb films on the Si(111) surface have been extensively studied due partly to the formation of an abrupt interface based on the low mutual solubility of Pb and Si.[1] Traditionally, this ideal interface has played the role of a model system to understand fundamental aspects of metal-semiconductor interfaces such as the Schottky barrier formation.[2–6] However, recent extensive researches on Pb ultrathin films on Si(111) have attracted renewed interest due to the electron quantization[7] and its consequences on various physical properties such as superconductivity,[8] surface diffusion,[9] and surface chemical bonding[10] as well as the growth mode of the films themselves.[11–15]

On the other hand, as a wetting layer or the interfacial layer between Pb films and the Si(111) substrate,[13] the dense Pb overlayer plays an important role, for example, to govern the electron scattering at the interface, which affects crucially the electron-quantization condition.[15–17] Moreover, the dense Pb overlayer itself exhibits a very complex and interesting phase evolution, which was, at sufficiently low temperature, shown to be the realization of the theoretical model of "devil's staircase (DS)."[18,19] In the DS phase diagram, two competing long-range orders with different densities produce an enormous variety of *linear* phases within a very small coverage window. In the case of Pb/Si(111), the $\sqrt{7} \times \sqrt{3}$ structure of 1.2 monolayer (ML) [Fig. 1(d)][22,23] and dense $\sqrt{3} \times \sqrt{3}$ of 1.33 ML [Fig. 1(b)] were suggested as the competing orders and the other phases with large commensurate unit cells are constructed by the linear combination of the two phases.[18] What makes the phase landscape more complicated is that the DS phases are not stable above 150–300 K to transit into phases with hexagonal or striped domain walls, which were called as hexagonal or striped incommensurate phases (HIC or SIC) [see Fig. 1(e)].[21,24–26] The HIC and SIC phases were suggested to be composed of dense $\sqrt{3} \times \sqrt{3}$ domains surrounded by domain walls with a $\sqrt{7} \times \sqrt{3}$-like

structure.[24] At a higher temperature around 270–350 K, all these complicated phases transit into the 1×1 or disordered phase, where all domain walls and superstructures disappear [Fig. 1(e)].[21,24] However, the detailed local bonding and structural aspects at the interface during this complex phase evolution have not been disclosed and the origin of the temperature-induced phase transition is not clear.[24]

In this work, we focus on the changes in the local structure and the bonding configuration in the dense Pb overlayers on Si(111) during the phase evolution as functions of coverage and temperature. We apply core-level photoelectron spectroscopy in combination with low-energy-electron diffraction (LEED) (Refs. 27 and 28) to the Pb coverage up to 1.3 ML at 200–400 K. Pb core-level spectra indicate that all these phases have two distinct bonding configurations for Pb atoms. The majority and the minority configurations can be related to the on-top (T1) and the hollow sites, respectively, from the structure models proposed previously.[18,20,22,23] Si surface-core levels also exhibit two different Si sites, which can also be explained within the present structural models,[18,20,22,23] by the difference among on-top sites caused by hollow-site adatoms. The temperature-induced phase transition from $\sqrt{7} \times \sqrt{3}$ to 1×1 exhibits no significant changes in the Pb core level but a small noticeable change in the Si core level. These behaviors lead to a microscopic explanation of the phase transition.

II. EXPERIMENT

A Si(111) wafer, miscut by $2°$ toward $[11\bar{2}]$, was flash heated up to 1470 K repeatedly to get a clean surface and then postannealed at 1123 K carefully to get a regular array of steps and terraces with a well-ordered 7×7 reconstruction.[29] The slightly miscut substrate with limited terrace widths or higher anisotropy is helpful in avoiding a mixture of triple rotated domains.[30] After the cleaning procedure, Pb was deposited onto the substrate held at 500 K
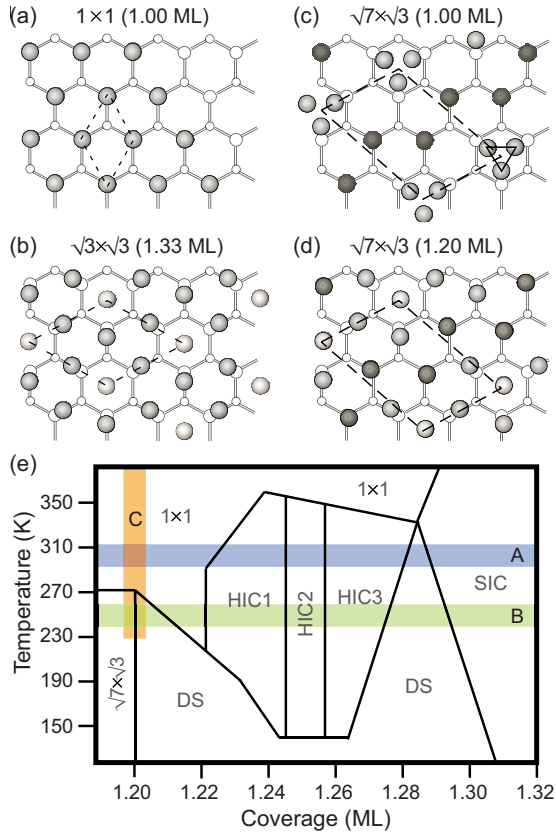
FIG. 1. (Color online) Schematics of structure models for the representative surface phases of Pb/Si(111). (a) The 1×1 phase at 1 ML (Ref. 20), (b) $\sqrt{3} \times \sqrt{3}$ at 1.33 ML (Refs. 18 and 20), (c) $\sqrt{7} \times \sqrt{3}$ at 1.0 ML (the trimer model) (Refs. 20 and 21), and (d) $\sqrt{7} \times \sqrt{3}$ at 1.2 ML (Refs. 18, 20, 22, and 23). Large (small) open circles denote the first- (second-) layer Si atoms and lager filled circles with different contrasts Pb atoms in different registries. (e) Phase diagram of the dense Pb/Si(111) system taken from Ref. 24, where the 1×1 phase over 1.2 ML was assigned as a disordered phase. The wide stripes (A, B, and C) indicate the phases probed in the present work.

using an effusion cell and the surface was postannealed at the same temperature to achieve a better surface ordering. The sample was then cooled down to 230–300 K for LEED and photoemission measurements, where various orderings occur. By varying the deposition time, we got a systematic series of uniform diffraction patterns from the submonolayer phase to the $14 \times \sqrt{3}$ phase of about 1.28 ML.[30] Since this phase formation at an elevated temperature involves the desorption of Pb, the deposition time does not linearly depend on the actual Pb coverage. We estimate the coverage of Pb roughly by the intensity of Pb $5d$ with the reference of the well-known $\sqrt{3} \times \sqrt{3}$ phase formed at a different temperature and at about 1/3 ML. Since different phases with proximal Pb coverages can easily coexist on the surface,[18] the uniform phase formation is important for an area-averaging spectroscopy study. We found that the direct resistivity heating, which flows the current through the sample, is far from being ideal in this respect due probably to the temperature gradient over the surface. In order to heat the sample more uniformly in the low-temperature range (300–500 K), we applied the
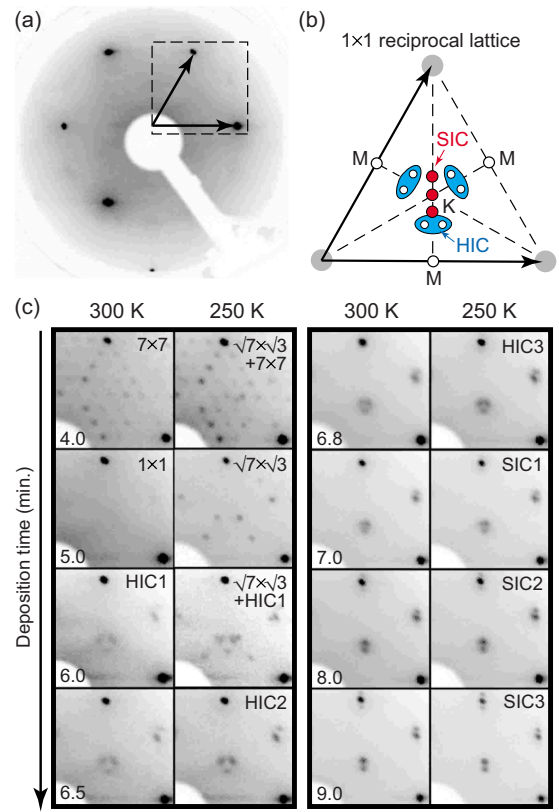
FIG. 2. (Color online) (a) LEED pattern with the beam energy of 82 eV for the 1×1 phase. (b) Schematic for the boxed area in (a) to identify the satellite spots shown in (c). (c) Enlarged LEED patterns of that boxed area for different Pb deposition times at 250 and 300 K.

indirect heating using a resistive heater built into the sample holding plate.

Photoelectron spectroscopy measurements were performed using synchrotron radiation from the soft x-ray undulator beamline 8A1 at Pohang Accelerator Laboratory. The end station was equipped with a high-resolution electron analyzer (SES-2002, Gammadata, Sweden) and a LEED optics. The overall instrumental energy resolution, defined by the photon beam and the electron analyzer, was set better than 20 meV. The sample temperature was controlled from 200 to 400 K during the measurements using liquid nitrogen and the feedback-controlled heater. For an unambiguous identification of surface components in Si $2p$, we used various photon energies and emission angles, which provide the varying surface sensitivity through the change in the photoelectron mean-free path. The photon energy ($h\nu$) used was 100–150 eV.

III. RESULTS AND DISCUSSION

A. Coverage dependence

Figure 2 shows the LEED patterns at two different temperatures of 250 and 300 K with different Pb deposition times. At 300 K, the 7×7 spots gradually diminish as the Pb coverage increases and turn into a 1×1 pattern with no su-

perstructure spots at the deposition of 5 min [Figs. 2(a) and 2(c)]. From about 6–7 min, weak split-off spots with a three-fold symmetry appear as centered on the $\sqrt{3} \times \sqrt{3}$ positions [K points of the 1×1 unit cell indicated in Fig. 2(b)]. This set of spots is composed of three rather elongated features but each one can barely be resolved into two spots as schematically shown in Fig. 2(b). The separation of the elongated features shrinks gradually as the deposition time increases until the diffraction features with a distinct symmetry appear at 8 min. Above 7 min, the almost merged triple spots evolve into a set of linearly spilt spots [Fig. 2(b)]. The splitting between these spots increases with the coverage but no further change is noticed above 9 min. While the triply degenerated spots correspond to the HIC phases of the phase diagram, the linearly split spots are assigned as the high-coverage DS phases. For the 9-min deposited surface, the superstructure-spot splitting can rather reliably be measured, which makes it possible to assign the phase as $14 \times \sqrt{3}$. This phase belongs to the DS phase diagram with a coverage of 1.28 ML as composed of two $\sqrt{7} \times \sqrt{3}$ and six $\sqrt{3} \times \sqrt{3}$ units. However, since the distinction between the high-coverage DS phases and the SIC phases is not sufficiently clear, we call all phases with the linearly spilt LEED spots as SIC phases for simplicity.

At a slightly lower temperature of 250 K, the evolution of LEED patterns is very much consistent except for the appearance of a $\sqrt{7} \times \sqrt{3}$ pattern at around 5–6 min. This pattern develops well without any noticeable mixing with other spots at about 5 min, which corresponds to the 1×1 phase at 300 K. This clearly indicates that there is a phase transition between the $\sqrt{7} \times \sqrt{3}$ and the 1×1 phases. This transition is found to be completely reversible.

Figure 3 shows the high-resolution Pb $5d_{5/2}$ spectra taken for the series of phases at 250 K. All the spectra in Fig. 3 are normalized by the peak intensity to show the line-shape change more clearly. Since the coverage change is smaller than 0.1 ML (1.2 ML at 5 min and 1.28 ML at 9 min according to the structure model proposed),[18] the variation in the total intensity is not significant. The spectra exhibit apparently asymmetric shapes with a shoulder feature and a long asymmetric tail at the high-binding-energy side. The tail structure is due to the inelastic scattering of photoelectrons, generating electron-hole pairs, which reflects the metallic nature of the surface. The two-dimensional metallic surface states of the dense Pb overlayers were characterized in detail recently by our group.[30] This line shape is very consistent over the whole coverage range probed here with little coverage dependence. In principle, this behavior is not beyond one's expectation because (i) the Pb coverage difference between the highest and the lowest phases is only 6% and (ii) no drastic change in local structures is expected in the structure models.[18,20,22,23] That is, within the DS model, the same building block structures are persistent while mainly the lateral arrangement of the building blocks changes.

The weak but discernible shoulder at the high-binding-energy side indicates rather unambiguously that there exist at least two different components with different binding energies and intensities. As for the $\sqrt{7} \times \sqrt{3}$ phase, the two components were more clearly resolved at a lower temperature due to the reduced thermal broadening.[31] We analyzed the
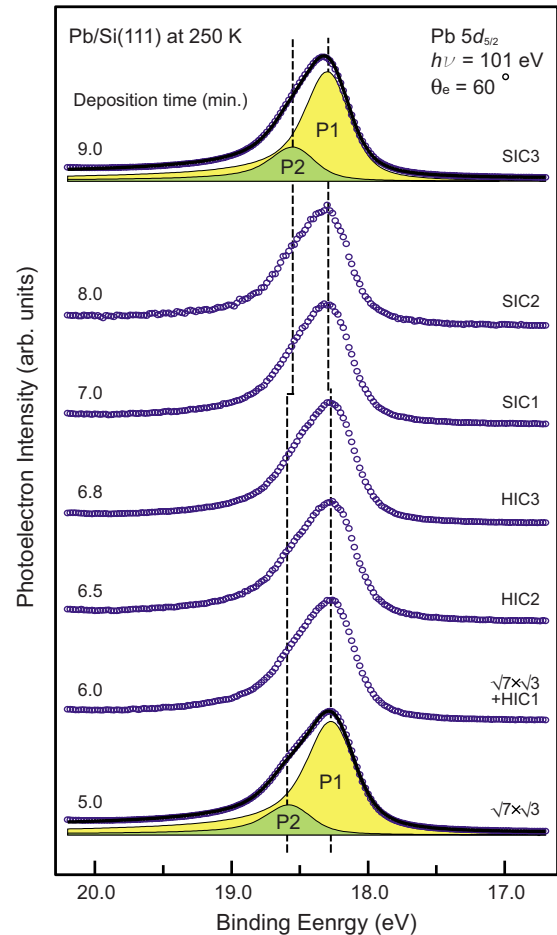
FIG. 3. (Color online) Pb $5d_{5/2}$ photoelectron spectra for Pb/Si(111) at 250 K. From the bottom to the top, the deposition time of Pb was changed from 5 to 9 min. The corresponding LEED patterns are denoted as assigned in Fig. 2(c). All spectra were taken with an $h\nu$ of 101 eV at an emission angle of 60° from the surface normal. The decompositions by the standard curve-fitting analysis are shown for two different coverages with well-defined LEED patterns. The results of the fits (solid lines) are overlaid onto the raw data (dots).

Pb $5d$ spectra by a standard least-squares fitting procedure with the Doniach-Sunjic line shape for metallic systems, which incorporates Lorentzian and Gaussian functions along with the asymmetry due to the inelastic scattering. The Lorentzian width is optimized to be 0.20 ± 0.02 eV, while the asymmetry parameter to be 0.13. Since the apparent spectral resolution is not sufficient in the present measurement, the peak positions of the minor component are not uniquely determined, but a consistent fitting can be performed for the whole spectra with the aid of the previous higher resolution data for the $\sqrt{7} \times \sqrt{3}$ phase.[31] The dominating $P1$ component and the higher-binding-energy $P2$ component, which explain the shoulder in raw spectra, have an energy splitting of 0.25–0.32 eV (see Table I for the detailed fitting parameters). The energy difference between $P1$ and $P2$ gradually decreases as the coverage increases while the relative intensity ratio is 1:4 ($P2$:$P1$) on $\sqrt{7} \times \sqrt{3}$ but slightly decreases to 1:3 on the $14 \times \sqrt{3}$ surface.

TABLE I. The major curve-fitting parameters for the Pb $5d_{5/2}$ spectra shown in Fig. 3. The binding energy (BE), the Gaussian width (GW), and the normalized intensity (I) of each component are given. The Lorentzian width is optimized to be 0.20 ± 0.02 eV.

Phase	Comp.	BE (eV)	GW (eV)	I
$14 \times \sqrt{3}$	P1	18.27	0.25	0.76
	P2	18.52	0.25	0.24
$\sqrt{7} \times \sqrt{3}$	P1	18.27	0.26	0.81
	P2	18.59	0.26	0.19

The two components of Pb $5d$ indicate that there exist two distinct bonding configurations for Pb adsorbates. Within the structure model,[18,20,22,23] these may correspond to the adsorbates on nearly T1 sites and those on hollow sites (so-called H3 or T4 depending on the registry with the second Si layer).
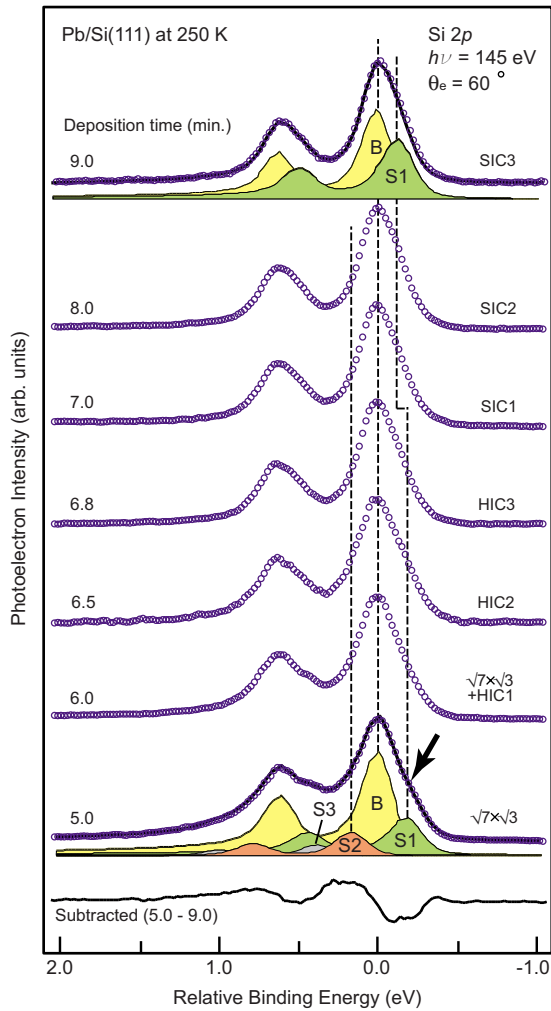
FIG. 4. (Color online) Si $2p$ photoelectron spectra for the Pb dense phases at 250 K shown in Fig. 2. All spectra were taken with an $h\nu$ of 140 eV at a grazing emission angle of 60°. The subtracted spectrum, between the 5 and 9 min spectra, is drawn to show the existence of the increase (decrease) in the S1 (S2) component at high coverage.

TABLE II. The major curve-fitting parameters optimized for the spectra (5 and 9 min) shown in Fig. 4. The surface-core-level shift (SCLS), binding-energy shift from the bulk component B, the GW, and the relative intensity ratio (I_{rel}) to B of each component are given. The Lorentzian width is optimized to be 60 meV.

Phase	Comp.	SCLS (eV)	GW (eV)	I_{rel}
$14 \times \sqrt{3}$	B	0	0.14	1.00
	S1	−0.14	0.17	0.73
$\sqrt{7} \times \sqrt{3}$	B	0	0.16	1.00
	S1	−0.18	0.17	0.38
	S2	0.17	0.18	0.25
	S3	0.38	0.18	0.11

The ratio between these two sites (hollow vs on top) varies from 1:5 to 1:3 from the $\sqrt{7} \times \sqrt{3}$ phase at 1.2 ML to dense $\sqrt{3} \times \sqrt{3}$ at 1.33 ML (1:3.2 for the $14 \times \sqrt{3}$ phase at 1.28 ML with two $\sqrt{7} \times \sqrt{3}$ and six $\sqrt{3} \times \sqrt{3}$ units). These values are qualitatively consistent with the observed intensity ratio between $P2$ and $P1$. For the trimer (1.0 ML) model of $\sqrt{7} \times \sqrt{3}$, there are no adatoms on hollow sites but the trimers and monomers of Pb on basically on-top sites instead [Fig. 1(c)]. One may still attribute the $P1$ and $P2$ components to the Pb trimers and monomers. Then, the corresponding population ratio should be 1:1.5 deviating significantly from the experiment. Since the measured intensity ratio is not uniquely determined due to the uncertainty of the curve fitting, the distinction between the structure models may be not conclusive enough here. However, our previous analysis of the surface band structure and our own coverage estimation by the Pb $5d$ intensity do not favor the 1.0 ML model.[30] More importantly, the 1.0 ML model cannot easily explain the consistent Pb $5d$ line shape for the high-coverage phases since this model requests a distinct bonding configuration, that is, an extra Pb $5d$ component, for the extra Pb adsorbates beyond 1.0 ML. Note also that the first-principles calculation indicated that the trimerization is energetically unfavorable.[20,23] The limitation of the 1.0 ML model will become more obvious in the study of the phase transition into the 1×1 phase as discussed below.

Si $2p$ spectra for the same coverage series as those in Figs. 2 and 3 are shown in Fig. 4. The line shape of Si $2p$ is so sharp that the previous photoemission study assigned only single spin-orbit doublet for this coverage range.[32] However, the higher-resolution data here make it obvious that there exist extra surface-related components. In the raw spectra, one can already notice the shoulder feature at the low-binding-energy side of the main peak (see the arrow). More detailed line shape is revealed by the curve-fitting analysis as partly shown in the figure. The curve-fitting analyses were performed for a set of spectra for a given coverage with different surface sensitivities (at different photon energies and emission angles) in order to unambiguously assign surface components.[33–35] The fitting shows two surface components S1 and S2 for the $\sqrt{7} \times \sqrt{3}$ phase with the surface-core-level shifts of −0.18 and 0.17 eV, respectively (see Table II for the detailed fitting parameters). The existence of the third

component S3 with a marginal intensity at a higher-binding energy is not clearly confirmed since its intensity largely depends on the asymmetry parameter of the other components. Since both S1 and S2 components exhibit a similar dependence on the emission angle (data not shown here) and the high surface sensitivity, we assign both to surface components from the topmost Si layer. For a Si surface with a monolayer adsorbate overlayer in a unique bonding configuration, one would expect a huge Si 2p component for the topmost Si layer.[33] This is in qualitative contrast to the present case suggesting that the $\sqrt{7} \times \sqrt{3}$ surface has Si surface atoms in, at least, two different bonding configurations.

As the coverage increases, the S1 component exhibits a gradual increase in intensity and binding energy while S2's intensity decreases. The $14 \times \sqrt{3}$ phase (SIC3) has the S1 component with an energy shift of −0.14 eV (Table II). In particular, the intensity increase is significant. This change is obvious even without the curve fittings as manifested by the subtraction of the low- and high-coverage spectra shown in the figure. That is, the surface Si atoms represented by S1 (S2) undergo a systematic increase (decrease) in their population during the phase evolution.

In the present structure model of the DS phases,[18,20,22,23] the low-density $\sqrt{7} \times \sqrt{3}$ structure has two slightly different Si bonding configurations: T1 and the deviated T1 site (T1′) (see Fig. 1). The T1′ site is generated by the hollow-site adatoms distorting the neighboring T1 sites. In contrast, the high-density $\sqrt{3} \times \sqrt{3}$ phase has only a unique one: the T1′ site with the increase population of the hollow-site adatoms. In both 1.0 and 1.2 ML models of $\sqrt{7} \times \sqrt{3}$, the population ratio of the two Si sites (T1 vs T1′) is 2:3 in quantitative accord with the intensity ratio of S2:S1 (see Table. II). This interpretation attributes the S1 (S2) component to the T1′ (T1) site. The binding-energy difference then suggests that the hollow-site Pb adatoms provide a more electron-rich environment for the Si atoms bonded to the adatoms on T1′ sites. The increase in S1 can be understood from the fact that the portion of the local $\sqrt{3} \times \sqrt{3}$ structure increases with the coverage, which, in turn, increases the population of the T1′ sites. The present result indicates clearly that the interfacial bonding configuration evolves systematically during the DS phase evolution, which is compatible with the present structure models.[18]

B. Temperature dependence

Temperature-dependent phase transition is one of the interesting issues within the complex phase diagram since all the DS phases transform into domain-wall phases of HIC or SIC and eventually to a 1×1 or disordered phase. It was suggested that the phase change between the DS phases and the HIC or SIC phases can be understood from the domain-wall rearrangement, where the domains are $\sqrt{3} \times \sqrt{3}$ phases and the domain walls are $\sqrt{7} \times \sqrt{3}$.[24] In particular, the HIC phase has hexagonal domain walls instead of linear ones found in DS and SIC phases. However, the atomic structure of the 1×1 phase as well as the origin of the transition is unknown.

The LEED patterns in Fig. 5(a) show the temperature de-
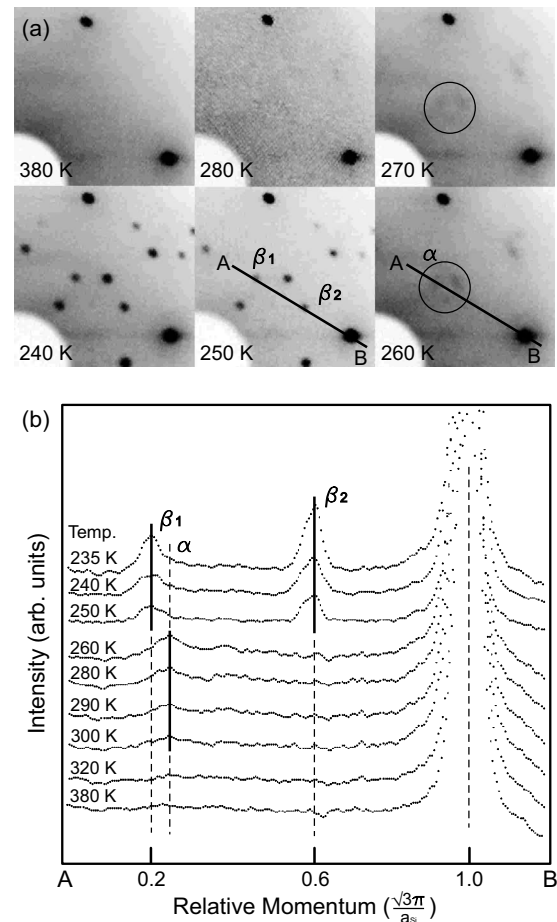
FIG. 5. (a) LEED patterns from the surface with the Pb deposition of 5 min taken at 84 eV [for the boxed area in Fig. 1(a)] for different temperatures indicated. (b) The line profiles from A to B are shown in (a).

pendence from the $\sqrt{7} \times \sqrt{3}$ phase at 240–380 K. Above 240 K, three phases are observed. First, the $\sqrt{7} \times \sqrt{3}$ diffraction pattern (with $\beta 1$ and $\beta 2$ spots) appears from 240 to 255 K, while only 1×1 spots are seen above 270 K. However, between two phases, very weak and fuzzy satellite spots (α) are observed. The intermediate phase looks very similar to the HIC phase. The line profiles given in Fig. 5(b) indicate that the $\sqrt{7} \times \sqrt{3}$ order decreases gradually as the temperature increases. The HIC-like order also decays gradually until it disappears completely at 380 K. This behavior is qualitatively consistent with the phase transitions of DS phases into HIC and 1×1 (disordered) phases and with the higher transition temperature into the 1×1 phase for the HIC phases [see Fig. 1(e)].[24] That is, the HIC-like spots can be due to the coexistence of minor domains of a higher density than the $\sqrt{7} \times \sqrt{3}$ phase.

Figure 6 shows the core-level spectra, which reflect the instantaneous local charge distributions on Si and Pb atoms for the $\sqrt{7} \times \sqrt{3}$ (lines) and 1×1 (symbols) phases at 250 and 300 K, respectively. The same data set for the high-coverage $14 \times \sqrt{3}$ phase with no phase transition at the given temperatures is shown for comparison. From the subtracted spectra for the $14 \times \sqrt{3}$ phase, both Si 2p and Pb 5d, one can estimate the pure temperature broadening, which is marginal for
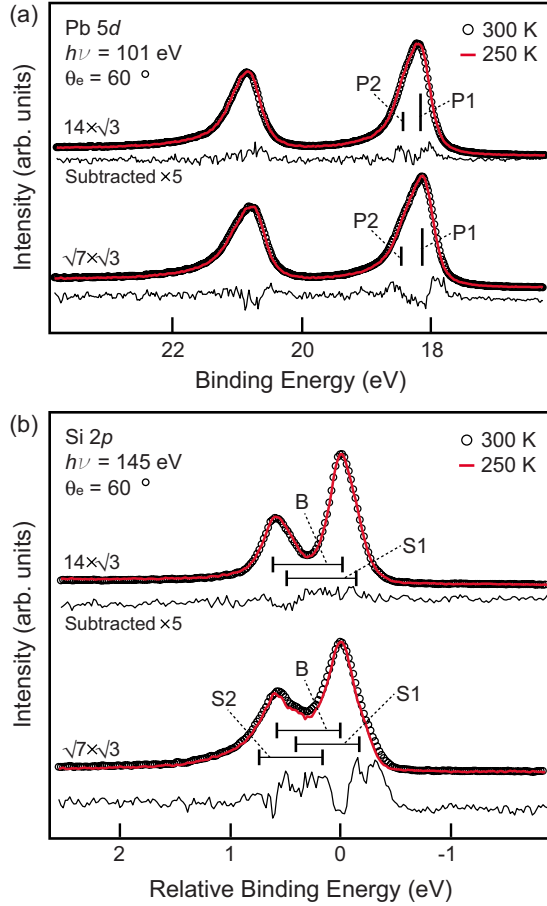
FIG. 6. (Color online) Temperature-dependent photoemission spectra for the $\sqrt{7} \times \sqrt{3}$ phase at 250 K (lines and dots) and 1×1 at 300 K (open circles). (a) Pb 5d and (b) Si 2p core levels taken at the same conditions as those in Figs. 3 and 4. For comparison, the spectra of the $14 \times \sqrt{3}$ (9 min) phase, exhibiting no phase transition, are shown together. The subtracted spectra after normalization by the peak intensity (300 K–250 K) are shown together, whose intensities are magnified by five times.

the 50 K difference. Although not conclusive, one may notice that the temperature-induced broadening of the spectrum of $\sqrt{7} \times \sqrt{3}$ is larger than that of $14 \times \sqrt{3}$, which might be related to the enhanced fluctuation of the 1×1 phase. In contrast, the subtracted Si 2p spectrum exhibits more pronounced changes. It indicates that mainly the S1 component (for the T1' configuration) has increased with the temperature increase for the $\sqrt{7} \times \sqrt{3}$ phase. These changes can trivially be confirmed by the curve-fitting analysis (not shown here). These results suggest that (i) the Pb overlayer configuration of hollow and on-top (T1 or T1') sites does not change significantly and (ii) the Si topmost layer becomes slightly more uniform in their bonding configuration with the increased population of the T1' configuration. It is notable that the 1×1 phase keeps two Pb bonding configurations of the $\sqrt{7} \times \sqrt{3}$ phase. One may also suspect that the 1×1 phase has an enhanced thermal fluctuation than the $\sqrt{7} \times \sqrt{3}$ phase.

The above results are apparently not compatible with the phase-transition model based on the 1.0-ML model for the $\sqrt{7} \times \sqrt{3}$ phase, where the T1-site 1×1 structure and the tri-

merization at low temperature is assumed (see Fig. 1).[21] The 1×1 phase in this model assumes a unique bonding configuration and a unique Pb 5d binding energy. Instead, a plausible scenario of the phase transition can be suggested based on the 1.2-ML model shown in Fig. 1(d). We suggest that the Pb adatoms in the hollow (H3 or T4) sites diffuse around rapidly on the surface. The diffusion can be the hopping between the H3 (T4) sites or the exchange diffusion between the H3 (T4) and T1 (T1') sites. Recently it was shown that the extra Ag adatoms on the $Si(111)\sqrt{3} \times \sqrt{3}$-Ag surface reside within the surface layer on the interstitial sites and diffuse very actively by the exchange diffusion.[36] While these diffusing adatoms are frozen into a superstructure at low temperature, the room-temperature phase looks just like the ideal $\sqrt{3} \times \sqrt{3}$ phase in LEED and scanning tunneling microscopy.[36] In the present case, the diffusing hollow-site adatoms would not be visible and only the host structure, 1×1, is detected. This scenario can explain two different Pb bonding configurations by the persistent adatoms on the hollow sites and the possible enhanced fluctuation by the adatom diffusion. The slightly increased population of the T1' configuration (about 15%) may also be explained since the diffusing Pb adatoms would affect more T1 sites and make the topmost Si layer more uniform.

IV. CONCLUSION

The evolution and the transition of phases in the dense Pb overlayers on the Si(111) surface have been studied by low-energy-electron diffraction and high-resolution core-level photoelectron spectroscopy using synchrotron radiation. The Pb 5d and Si 2p core-levels are measured for several representative phases in its devil's staircase phase diagram for the Pb coverage of 1.2–1.3 ML at 250 and 300 K.

Pb 5d photoelectron spectra are found to have two components indicating two distinct bonding configurations of Pb. These components can be related to the different Pb adsorption sites within the present structure models of hollow and on-top sites. In case of surface Si atoms, mainly two different bonding environments are revealed by surface Si 2p components for the low-density $\sqrt{7} \times \sqrt{3}$ phase. These are attributed to the Si surface atoms bonded with the Pb adsorbates on T1 and T1' positions. As the coverage increases, the minority site T1 converts to the majority one T1'. That is, the topmost Si layer has a unique bonding configuration in the high-coverage phase. This behavior can be understood from the present structure models since the high-coverage DS phases are dominated by the $\sqrt{3} \times \sqrt{3}$ phase with a unique surface Si bonding configuration (T1') due to the increased population at the hollow-site adatoms.

The temperature-dependent study confirms that the $\sqrt{7} \times \sqrt{3}$ phase undergoes a reversible phase transition into a 1×1 phase. This phase transition induces no significant change in Pb core levels with two different components. The simple structure model of 1×1 at 1.0 ML is thus denied. The Si 2p component for the T1' site increases slightly in the 1×1 phase. We suggest a phase-transition scenario based on these results, in which the local $\sqrt{7} \times \sqrt{3}$ structure with 1.2 ML Pb on hollow and on-top sites is more or less intact but

the Pb atoms in the hollow sites diffuse rapidly to prevent a long-range order. The present results emphasize the importance of the bonding with the Si substrate atoms in the phase evolution of dense Pb overlayers.

---

*yeom@yonsei.ac.kr

[1] G. Le Lay, M. Abraham, A. Kahn, K. Hricovini, and J. E. Bonnet, Phys. Scr. **T35**, 261 (1991).

[2] D. R. Heslinga, H. H. Weitering, D. P. van der Werf, T. M. Klapwijk, and T. Hibma, Phys. Rev. Lett. **64**, 1589 (1990).

[3] S. Hasegawa, X. Tong, S. Takeda, N. Sato, and T. Nagao, Prog. Surf. Sci. **60**, 89 (1999).

[4] Y. Miura, S. Fujieda, and K. Hirose, Phys. Rev. B **50**, 4893 (1994).

[5] R. T. Tung, Phys. Rev. Lett. **84**, 6078 (2000).

[6] H. H. Weitering, A. R. H. F. Ettema, and T. Hibma, Phys. Rev. B **45**, 9126 (1992).

[7] S. H. Chang, W. B. Su, W. B. Jian, C. S. Chang, L. J. Chen, and T. T. Tsong, Phys. Rev. B **65**, 245401 (2002).

[8] Y. Guo, Y.-F. Zhang, X.-Y. Bao, T.-Z. Han, Z. Tang, L.-X. Zhang, W.-G. Zhu, E. G. Wang, Q. Niu, Z. Q. Qiu, J.-F. Jia, Z.-X. Zhao, and Q.-K. Xue, Science **306**, 1915 (2004).

[9] L.-Y. Ma, L. Tang, Z.-L. Guan, K. He, K. An, X.-C. Ma, J.-F. Jia, Q.-K. Xue, Y. Han, S. Huang, and F. Liu, Phys. Rev. Lett. **97**, 266102 (2006).

[10] X. Ma, P. Jiang, Y. Qi, J. Jia, Y. Yang, W. Duan, W.-X. Li, X. Bao, S. B. Zhang, and Q.-K. Xue, Proc. Natl. Acad. Sci. U.S.A. **104**, 9207 (2007).

[11] K. Budde, E. Abram, V. Yeh, and M. C. Tringides, Phys. Rev. B **61**, R10602 (2000).

[12] M. Hupalo, V. Yeh, L. Berbil-Bautista, S. Kremmer, E. Abram, and M. C. Tringides, Phys. Rev. B **64**, 155307 (2001).

[13] M. Hupalo and M. C. Tringides, Phys. Rev. B **65**, 115406 (2002).

[14] Z. Zhang, Q. Niu, and C.-K. Shih, Phys. Rev. Lett. **80**, 5381 (1998).

[15] V. Yeh, L. Berbil-Bautista, C. Z. Wang, K. M. Ho, and M. C. Tringides, Phys. Rev. Lett. **85**, 5158 (2000).

[16] P. Czoschke, H. Hong, L. Basile, and T.-C. Chiang, Phys. Rev. Lett. **93**, 036103 (2004).

[17] D. A. Ricci, T. Miller, and T.-C. Chiang, Phys. Rev. Lett. **95**, 266101 (2005).

[18] M. Hupalo, J. Schmalian, and M. C. Tringides, Phys. Rev. Lett.

90, 216106 (2003).

[19] P. Bak, Rep. Prog. Phys. **45**, 587 (1982).

[20] T.-L. Chan, C. Z. Wang, M. Hupalo, M. C. Tringides, Z.-Y. Lu, and K. M. Ho, Phys. Rev. B **68**, 045410 (2003).

[21] I.-S. Hwang, S.-H. Chang, C.-K. Fang, L.-J. Chen, and T. T. Tsong, Phys. Rev. Lett. **93**, 106101 (2004).

[22] C. Kumpf, O. Bunk, J. H. Zeysing, M. M. Nielsen, M. Nielsen, R. L. Johnson, and R. Feidenhans'l, Surf. Sci. **448**, L213 (2000).

[23] S. Brochard, E. Artacho, O. Custance, I. Brihuega, A. M. Baró, J. M. Soler, and J. M. Gómez-Rodríguez, Phys. Rev. B **66**, 205403 (2002).

[24] S. Stepanovsky, M. Yakes, V. Yeh, M. Hupalo, and M. C. Tringides, Surf. Sci. **600**, 1417 (2006).

[25] J. Slezák, P. Mutombo, and V. Cháb, Phys. Rev. B **60**, 13328 (1999).

[26] O. Custance, I. Brihuega, J.-Y. Veuillen, J. M. Gómez-Rodríguez, and A. M. Baró, Surf. Sci. **482-485**, 878 (2001).

[27] K. Horikoshi, X. Tong, T. Nagao, and S. Hasegawa, Phys. Rev. B **60**, 13287 (1999).

[28] L. Seehofer, G. Falkenberg, D. Daboul, and R. L. Johnson, Phys. Rev. B **51**, 13503 (1995).

[29] J. Viernow, J.-L. Lin, D. Y. Petrovykh, F. M. Leibsle, F. K. Men, and F. J. Himpsel, Appl. Phys. Lett. **72**, 948 (1998).

[30] W. H. Choi, H. Koh, E. Rotenberg, and H. W. Yeom, Phys. Rev. B **75**, 075329 (2007).

[31] K. S. Kim, W. H. Choi, and H. W. Yeom, Phys. Rev. B **75**, 195324 (2007).

[32] J. A. Carlisle, T. Miller, and T.-C. Chiang, Phys. Rev. B **45**, 3400 (1992).

[33] C. J. Karlsson, F. Owman, E. Landemark, Y.-C. Chao, P. Martensson, and R. I. G. Uhrberg, Phys. Rev. Lett. **72**, 4145 (1994).

[34] S. W. Cho, K. Nakamura, H. Koh, W. H. Choi, C. N. Whang, and H. W. Yeom, Phys. Rev. B **67**, 035414 (2003).

[35] H. Koh, J. W. Kim, W. H. Choi, and H. W. Yeom, Phys. Rev. B **67**, 073306 (2003).

[36] H. Jeong, H. W. Yeom, and S. Jeong, Phys. Rev. B **76**, 085423 (2007); (unpublished).